Title: Evidence for Direct Suspension of Loessial Soils on the Columbia Plateau

J.F. Kjelgaard, D.G. Chandler, K.E. Saxton (retired)

Abstract:
Wind erosion modeling efforts, both field and wind tunnel studies, have traditionally focused on saltation-based processes for estimating dust emissions from high wind events. This approach gives generally good results when saltation-sized particles, 90 μm to 2 mm mean diameter, are prevalent on the exposed soil surface. The Columbia Plateau, located in north-central Oregon and south-central Washington, is a region with extensive loess deposits where up to 90% of sieved particles (by mass) are less than 100 μm mean diameter. During high wind events, large amounts of soil and fine particulate matter are suspended. However, field surfaces typically show little evidence of surface scouring or saltation, e.g. soil drifts or covered furrows. Velocity profile analysis of two high wind events and additional data from a third event show evidence of direct suspension process where saltation is not a major mechanism for eroding soil or generating dust emissions. Surface roughness heights are less than saltation roughness height estimates during peak wind speeds.

Keywords: wind erosion, dust emissions, PM_{10}, roughness height, friction velocity

Introduction

Wind erosion and dust emissions from arid regions cause land degradation, pose environmental health hazards, affect local, regional, and global climate patterns, and influence the earth's radiation/energy balance. Because of the dispersive nature of aeolian transport processes, suspension of particulate matter (PM) from relatively small emission source areas can impact much greater surface areas downwind. Understanding the emission and transport processes for soil and mineral particles with mean diameters < 60 μm (dust) is especially important to agricultural air quality issues because these soil particles can contain significant amounts of soil nutrients (Zobeck and Fryrear, 1986), contaminants (Pye, 1987), and pose respiratory hazards from particles < 10 μm mean aerodynamic diameter (PM_{10}) (U.S. Environmental Protection Agency, 1990).

Entrainment of dust particles (and subsequent suspension) is controlled by several factors including: 1) impacts by rolling or bouncing particles (saltation), 2) momentum drag produced by the wind, 3) aerodynamic lift, and 4) vehicle or pedestrian traffic on an erosion area (Pye, 1987). A vast majority of the experimental and modeling work related to dust entrainment has focused on the role of saltation to generate dust emissions (e.g. Gillette and Walker, 1977; Borrmann and Jaenicke, 1987; Kind, 1992; Shao et al., 1993; Cahill et al., 1996; Houser and Nickling, 2001). Such an approach is logical when dealing with soils and sands where saltation layers are easily established. The saltating particles, with mean diameters generally between 70 to 500 μm, typically have smaller threshold shear velocities (u_{*t}) (Bagnold, 1941; Chepil, 1945; Zingg, 1953) and are less subject to cohesive forces that dominate the transport of smaller particles (Sagan and Bagnold, 1975; Iversen et al., 1976).

Wind erosion/dust emission research has therefore primarily focused on the saltation process as being necessary to entrain smaller dust particles via surface collisions and particle abrasion (Shao, 2001). Field evidence of saltation has been documented several ways including 1) direct observation (e.g. Bagnold, 1941), 2) analysis of sediment trap data (e.g. Gillette and Walker, 1977; Nickling, 1983; Leys and McTainsh, 1996), and 3) particle collisions with impact recording devices such as Sensits® and saltiphones (e.g. Stout, 1990; Gillette et al., 1997; Sterk and Spaan, 1997). However, these methods have limitations when dealing with soils dominated by dust-sized particles including 1) lack of a highly defined saltation layer during high wind events, 2) low efficiency of sediment traps for small particles, and 3) low sensitivity of impact sensors to small particles.

An alternative method to document saltation is by analysis of wind velocity profile modification (Owen, 1964; Gillette et al., 1996; Gillette et al., 1998). Particle mass flow near the eroding surface increases drag and friction velocity (u_*) with increasing wind speed. Gillette et al. (1997; 1998) presented field data that demonstrated modified velocity profiles due to saltation as suggested by Owen (1964) and documented by several wind tunnel studies (Bagnold, 1941; Zingg, 1953; White, 1982; Anderson and Haff, 1991). Raupach (1991) presented a related analysis of saltation layer effects on surface roughness parameters and proposed a formula for estimating a saltation roughness height (z_{0s}).

Much less theoretical and applied research has focused on aerodynamic lift as a mechanism for dust generation and suspension. This was likely the result of early wind tunnel studies which showed that particles smaller than 80 μm required much higher wind speeds to provide adequate momentum drag and/or aerodynamic lift to initiate particle movement (e.g. Bagnold, 1941). Loosmore and Hunt (2000) recently examined the suspension of fine particles (Arizona Test Dust: alumino-silicate particles < 10 μm, with a modal particle size of 5 μm) from a uniform dust bed with a small laboratory wind tunnel. They found that dust emission was continuous throughout their experiments, although particle concentrations quickly dropped from relatively high levels to below visible levels once wind tunnel runs commenced, similar to other experiments they cite.

The Columbia Plateau, located in north-central Oregon and south-central Washington, is a region with extensive loess deposits where up to 90% of particles (by mass) may have diameters less than 100 μm (U.S. Department of Agriculture, 1967). Wind erosion and dust entrainment has been monitored for several years (Saxton, 1995; Saxton et al., 2000). Stetler and Saxton (1996) observed that significant soil deposition was rarely observed along field boundaries, fence lines, or roads except for stable, prehistoric dunes scattered throughout the area. In addition, little evidence of surface scouring or large-scale deposition was seen in fields after high wind events and analyses of horizontal soil transport and vertical dust flux did not follow expected trends based on conventional soil transport models. Use of piezoelectric impact sensors has been limited due to the small particle sizes found on the soil surfaces (Stockton, personal communication; Stout and Zobeck, 1997). These observations strongly suggest that minimal saltation occurs during wind erosion on these regional soils and entrainment by direct suspension processes is dominant.

The objective of this paper is to present field evidence of dust entrainment by direct aerodynamic suspension in the absence of significant saltation. We propose to examine whether saltation was occurring by utilizing actual u_* and z_0 measurements. Wind velocity data were analyzed in conjunction sediment trap particle size analysis and limited continuous PM_{10} measurement from individual events. The data were from high wind dust storms on the Columbia Plateau of Washington state, a region where prevalent farm practices expose large areas of bare soils to high winds.

Analysis

Wind velocity profile analyses provide information on surface parameters such as friction velocity (u_*) and roughness height (z_0). These parameters can confirm the effect of saltation (Owen, 1964; Gillette et al., 1997; Gillette et al., 1998) due to the additional particle load on the lower part of the velocity profile. The saltating particles produce more near-surface drag for the wind to overcome and increase u_* and "saltation" roughness height (z_{0s}) (Raupach, 1991).

The coefficient of drag (C_d) for a surface may be defined:

$$C_d = \left(\frac{u_*}{u_z} \right)^2 \quad (1)$$

where u_z is wind speed (m s^{-1}) at a particular reference height z. A constant ratio of u_*/u_z under varying wind velocities indicates that neither C_d nor z_0 are changing. This is demonstrated

graphically if a plot of u_* versus u_z results in a linear relationship of constant slope (Gillette et al., 1997; Gillette et al., 1998) and indicates no saltation is occurring.

The logarithmic wind profile for neutral conditions can be described by the equation:

$$u_z = \frac{u_*}{k}\ln\left(\frac{z}{z_0}\right) \qquad (2)$$

where k is Von Karman's constant (0.4). Both u_* and z_0 were determined using equation (2) by regression analysis of several velocities versus the natural log (ln) of the corresponding anemometer heights for an individual time-step. The u_* term was the product of the linear regression slope and von Karman's constant k (0.4) and z_0 was the exponential of the slope intercept divided by the negative of the regression slope.

In order to verify stability conditions, a simplified Richardson's number (Ri) was calculated based on wind speed and temperature measurements at two heights (Kaimal and Finnigan, 1994):

$$Ri = \frac{\left(g/T\right)\left(\gamma_d + \partial T/\partial z\right)}{\left(\partial u/\partial z\right)} \qquad (3)$$

where g is the gravitational constant (9.81 m s^{-2}), T is mean temperature (ºK), γ_d is a constant (-0.0098 ºC m^{-1}), and ∂T (ºK) and ∂u (m s^{-1}) are the temperature and wind speed differences over the distance between measurements, ∂z (m). The stability regimes were determined using the Ri intervals found in Thom (1975).

Ideally, conditions for determination of valid u_* and z_0 values require a high degree of linearity (e.g. coefficient of correlation (r^2) ≥ 0.95 or greater) depending on the number of measurement heights comprising the individual wind velocity profile (Stull, 2000). No corrections were made for roughness displacement height, due to bare, fallow conditions, or atmospheric stability, due to strong surface winds. At least two averaging times and/or height intervals within the velocity profile were examined for each event. For 10-minute averages, several wind velocities from 0.1 to 5 m were used. When 1-minute averages of velocity measurements were available, wind velocities from the two lowest anemometers were utilized to calculate a separate set of u_* and z_0 values. It was felt that 1-minute averages, though unconventional, were capable of displaying possible short-term, surface-level effects that might occur in the wind velocity profile. Data for analysis were selected based on sustained high wind speeds of 5 m s^{-1} or 6.4 m s^{-1} at heights of 2 m or 3 m, respectively, and screened for wind direction, increasing wind speed with height, debris influencing lower anemometer heights, and general operation.

Change in u_* due to saltation may be indicated by a change in z_0. Estimates of z_{0s} (roughness height when a saltation layer is present) were made with the equation (Raupach, 1991):

$$z_{0s} = \left(A\frac{u_*^2}{2g}\right)^{1-\sqrt{r}} z_{0u}^{\sqrt{r}} \qquad (4)$$

where A is a constant with a suggested field value between 0.2 and 0.3 (following Raupach, A = 0.22 was used for our calculations), $u_*^2/2g$ proportions the additional roughness height to a

simplified, ballistic path followed by a saltating particle, and z_{0u} is an undisturbed roughness height determined when no saltation is occurring. The √r factor is defined as:

$$\sqrt{r} = \frac{u_{*t}}{u_*} \qquad (5)$$

where u_{*t} is the threshold friction velocity (m s^{-1}). The value u_{*t} refers to the wind friction velocity required to initiate particle movement. This was estimated for the representative modal surface soil particle diameter (D_p) using the formula of Marticorena and Bergametti (1995):

$$u_{*t}(D_p) = 0.129 \frac{\left[\frac{\rho_p\, g\, D_p}{\rho_a}\right]^{0.5} \left[1 + \frac{0.006}{\rho_p\, g\, D_p^{2.5}}\right]^{0.5}}{\left[1.928\left(a\, D_p^{x} + b\right)^{0.092} - 1\right]^{0.5}} \qquad (6)$$

where D_p is the particle diameter (cm), ρ_p is particle density (2.65 g cm^{-3}), g is gravitational constant (980 cm s^{-2}), ρ_a is air density (0.00123 g cm^{-3}), and *a* (1331), *b* (0.38) and *x* (1.56) are non-dimensional constants.

To aid in comparing z_{0s} values with other observations and models, equation (4) may be rearranged to yield a non-dimensional variable C (Raupach, 1991):

$$C_{obs} = \frac{z_{0-obs}}{\left(\frac{u_*^{\,2}}{2g}\right)} \qquad (7)$$

and

$$C_{est} = A^{1-\sqrt{r}} \left(\frac{z_{0u}}{u_*^{\,2}/2g}\right)^{\sqrt{r}} \qquad (8)$$

where C_{obs} and $z_{0\text{-}obs}$ are field-based observed conditions and C_{est} is an estimated value for a realistic set of A, z_{0u}, and u_{*t} parameters. If saltation is occurring during a field experiment then $C_{obs} \geq C_{est}$ and $z_{0\text{-}obs} \geq z_{0s}$. In this paper, the $z_{0\text{-}obs}$ represents roughness heights determined during dust storms.

Materials and Methods

The Columbia Plateau region of central Washington is typified by numerous large fields in dryland wheat production managed in a crop-fallow rotation (i.e. one year the field is planted/harvested and the next year it is left dormant and bare). The predominant soil type is Ritzville silt loam (Andic Aridic Haplustoll), a mixture of loess, volcanic ash particles, and very low (< 1.0%) organic matter. As such, the primary particles in the soil do not include a large population of saltators or similarly sized aggregates. The bare fallow fields are subject to a variety of machinery operations such as disking, to incorporate organic residues, and rod-weeding to reduce parasitic water-use by weeds and develop a soil surface moisture barrier. Seeding operations for winter wheat occur in August and September when surface soils are typically dry and strong west and south winds are likely. Each of these farming operations progressively breaks down the surface soil structure and aggregates which results in large areas being highly susceptible to wind erosion.

Three relatively level, fallow fields were selected for instrumentation. Large field sizes allowed for ample fetch (300+ m) in the predominant wind directions (west and south). The instrumented sites were typically changed every year. Therefore, the following convention was used to identify fields during different years: R-99, the 1999 site, W-01, the first 2001 field site, and IS-01, a second field site of 2001. Both R-99 and W-01 had undergone deep furrow seeding operations just prior to the high wind events. The location of the W-01 site was 1 km east of several large, vegetated sand dunes (Sand Dunes State Park, Washington). The IS-01 site was on a research field site selected for ongoing intensive wind erosion and dust emission field studies. This site was a 9 ha corner of a larger, 300+ ha field that was harvested in the summer of 2001. The field containing the IS-01 site had been disked once prior to 09/25/01, leaving approximately 50% crop residue, both standing and flat. The 9 ha zone was disked once more before 10/12/01, leaving approximately 30% predominantly flat residue.

Meteorological stations for R-99 and W-01 sites consisted of the following components: cup anemometers at 5 heights (0.1 m, 0.75 m, 1.5 m, 3.0 m, and 5.0 m) (Model 014A , Met One Instruments, Grants Pass, Oregon); air temperature profile (0.1 m, 1.5 m, 5.0 m) with type T thermocouples (TCs); solar radiation (LI200X , LiCor Instruments, Lincoln, Nebraska); relative humidity/air temperature sensor (207 Probe, Campbell Scientific, Inc., Logan, Utah); tipping bucket rain gauge (TE525, Texas Electronics, Dallas, Texas); wind direction sensor (Model 025, Met One Instruments, Grants Pass, Oregon); datalogger (Model 21x, Campbell Scientific, Inc., Logan, Utah). Data were continuously recorded at 15-minute averages. Collection of 1-minute averages was started when wind speed at 3 m height exceeded 6.4 m s^{-1} for a period of 10 minutes. The averaging time returned to 15-minute intervals when winds at 3 m were less than 5.75 m s^{-1} for 15 consecutive minutes.

The IS-01 site included a slightly different array of meteorological sensors: cup anemometers at heights of 0.1 m, 0.5 m, 1 m, 2 m, 3 m and 5 m; fine-wire TCs at the same heights excluding 2 m; datalogger (Model 23x, Campbell Scientific Inc., Logan, Utah). Wind direction and relative humidity/air temperature sensors were at 2 m height. Additional instrumentation included soil temperature and heat flux information, radiation measurements, and rainfall monitoring. Frequency of data sampling was 0.1 Hz. Under normal conditions, 30-minute and 24-hour climate data were recorded. When wind velocity exceeded 5 m s^{-1} for 10 minutes at the 2 m level, surface temperature, relative humidity (RH), solar radiation, air temperature profiles and differences, and wind speed profiles were recorded every 10 minutes. Recording returned to normal increments when wind velocity became less than 5 m s^{-1} (at 2 m) for 15 consecutive minutes.

Event-averaged measurements of streamwise soil erosion and PM_{10} concentrations were made at the R-99 and W-01 sites via 12 clusters of BSNE traps (Fryear, 1986), a cluster contained five BSNEs at heights of 0.1, 0.2, 0.5, 1.0, and 1.5 m, and three high volume, constant-flow air samplers (General Metal Works, Village of Cleves, Ohio) with PM_{10} inlet heads deployed at heights of 1.5, 2.5, and 5.0 m. Dynamic PM_{10} concentrations at the IS-01 site were monitored at 10-minute intervals with two tapered element oscillating microbalance (TEOM) units (Model 1400ab, Rupprecht & Patashnick Co., Inc.; Albany, New York) fitted with 10 μm particle cut-off inlets. Inlets were placed at heights of 1 m and 3 m ($TEOM_{1m}$ and $TEOM_{3m}$). During field

installation of the TEOMs in the early part of October 2001, both units were monitored during calm wind periods to ensure similar readings.

Aggregate size distributions (ASD) for the Ritzville silt loam were determined to identify a representative surface particle size using two techniques: dry sieving and dispersed laser diffraction. Sieved soils were collected in 1999 from three separate fields and results averaged. Samples were initially hand-sieved through a 4 mm screen to remove large aggregates. The remaining soil, approximately 75 g., was shaken sequentially through two stacks of eight-inch diameter, wire sieves for 10-minutes per stack. The sieve shaker (RoTap®, W.S. Tyler, Mentor, Ohio) was operated to oscillate sieves horizontally at 5 Hz and tap the sieve stack at 2.5 Hz. Sieve openings of 2000, 1400, 1000, 710, 500, and 355 μm were part of the initial sieve stack. The remaining, finer-than-355 μm sample was then sieved through screens with openings of 250, 180, 125, 90, 63, and 45 μm. Sub-samples of the < 4 mm soil samples were taken with a small soil splitter, hand-sieved through a 250 μm standard sieve, and run through three-inch diameter sonic sieves (Gilson Company, Inc., Worthington, Ohio). Again, two stacks of sieve sizes were used; 150, 100, and 63 μm in the initial stack and 45, 30, and 10 μm in the sequential stack. A latex bag collected particles that passed the 10 μm sieve. The sonic sieve oscillated a column of air through the sieve stack at 60 Hz while alternately tapping the stack horizontally and vertically at 1 Hz.

The sonic sieve was also used to analyze ASD for BSNE catch from the 09/25/99 storm to examine particle size distribution and height relationships. Soil trapped by several BSNE samplers were bulked by sampler height and subsampled with a mechanical splitter. The subsamples were sieved with the same protocol as surface soils however sieve sizes of 100, 45, and 10 μm were utilized.

Laser diffraction particle size analyses were performed on 1999 and 2001 soil samples. The 1999 samples were pretreated to remove carbonates and organic matter, and dispersed in a sodium hexametaphosphate solution prior to analysis (i.e. strongly dispersed). The 2001 samples were run through a 125 μm wire sieve via a Ro-Tap® operated for 2 minutes. Samples from the finer-than-125 μm fraction were placed in de-ionized water and analyzed (i.e. weakly dispersed). The laser-sizer had particle size ranges of 0.01 to 800 um (Mastersizer S, Malvern Instruments, Inc., Southborough, Massachusetts).

Results

Meteorological data for three high wind dust events were analyzed. The first two events (09/25/99 and 09/25/01) were large regional storms resulting in several fatal vehicular accidents and numerous road closures. These large storms are observed to occur once every 1 to 5 years. The third event (10/12/01) was much smaller in scale, not as intense, and did not result in any regional road closures. Storms of that magnitude may occur several times a year.

Wind Velocity Profiles:

The first wind event analyzed occurred on September 25, 1999, from approximately 02:30 to 21:30 (PDT), with scattered periods of high winds a few hours before and after. A valid series of 1-minute averages for velocity profile analysis occurred from approximately 03:00 to 14:00 (PDT), when the strongest winds were blowing out of the southwest (232˚± 7˚ based on true north). The wind direction shifted at approximately 5:30, with prior winds from 197˚± 5˚. Following 14:00, and for a 40-minute period between 8:00 and 9:00, one or more of the anemometers measured zero velocity, indicating obstruction by a blowing weed. These periods were not included in the analysis. Event-averaged PM_{10} concentration was approximately 1500 μg m^{-3} at 1.5 m height determined by the high volume air sampler.

Average values, based on 10-minute data, of u_* and $z_{0\text{-obs}}$ were 0.631 ± 0.133 m s^{-1} and 0.005 ± 0.0006 m, respectively, with wind speeds between 4 to 12 m s^{-1} at 1.5 m height. Approximately 90% of the velocity profiles analyzed with Eq. 2 had regression coefficients (r^2) greater than 0.99 and average Ri was 0.002 ± 0.005, indicating neutral atmospheric conditions. For 1-minute results, all the profiles from approximately 3:00 am to 14:00, except for 40 minutes between 8:00 and 9:00, were used to calculate velocity profile slopes and intercepts. Plots of 10-minute and 1-minute u_* versus $u_{1.5m}$ are shown in Figs. 1a and 1b, respectively. Both plots show clear, linear response of u_* to increases in $u_{1.5m}$ with r^2 values of 0.98 and 0.91, respectively, and the 95% confidence intervals (dotted lines) indicate an excellent fit of the regression lines. Noting that the wind profile method may not produce precise values of z_0 (Gillette et al., 1998), an analysis of z_0 was also done following the method of Ling (1976); an identical value of $z_{0\text{-obs}}$ was produced, 0.005 m.

Wind velocity profiles from the second high wind event (09/25/01) were analyzed with quality checks identical to those done on the 1999 HWE data. High winds began at approximately 06:00 from the northeast which caused interference between the support tower and anemometers. By 09:15 winds had shifted to the southeast (from 164˚± 14˚ based on true north) and no tower interference was noted. After 13:00, winds were primarily out of the south (184˚± 10˚). Velocity profiles were analyzed using only four anemometers due to a faulty connection at the 0.75 m height. Precipitation late in the event (approximately 18:00 PDT) suppressed all erosion and dust production from the site. Therefore, a valid series of 1-minute averages for velocity profile analysis occurred from approximately 09:15 to 18:00 (PDT). Prevailing winds were from the south during the event. No evidence for substantial surface creep, saltation, or deposition was seen at the W-01 site immediately after the dust event ceased. Overall, the duration of the 09/25/01 event was several hours shorter than the ’99 wind event. However, the event-averaged PM_{10} concentration was approximately 2800 μg m^{-3} at 1.5 m height.

The 09/25/01 10-minute velocity data, utilizing anemometer heights from 0.1 to 5 m height, produced event-averaged u_* and $z_{0\text{-obs}}$ values of 0.426 ± 0.201 m s^{-1} and 0.001 ± 0.0006 m, respectively. Over 90% of the velocity profiles analyzed with Eq. 2 had regression coefficient of error (r^2) greater than 0.99 and average Ri was 0.009 ± 0.013, indicating neutral to near-neutral atmospheric conditions. The relatively low z_0 confirmed field observations that the winds were closely aligned with the planting furrows surrounding the meteorological tower. The plot of 10-minute and 1-minute averaged u_* versus $u_{1.5m}$ are shown in Fig. 2. The 1-minute calculations of u_* used velocity readings from 0.1 and 1.5 m, the two lowest operating anemometers. Linear

relationships between u_* and $u_{1.5m}$ are shown over the entire range of wind speeds (4 to 14 m s^{-1} at 1.5 m); r^2 was greater than 0.98 for both 10-minute and 1-minute data. Both plots showed narrow 95%-confidence intervals. The overall $z_{0\text{-}obs}$ value did not change when the velocity profiles were analyzed following Ling (1976).

The third high wind event occurred on 10/12/01 from approximately 06:00 to 23:30 (PDT). Wind velocities at 2 m height ranged between 4 to 14 m s^{-1}, predominantly out of the west and northwest. Data from the W-01 site was not analyzed due to failures of the 0.1 m and 0.75 m anemometers throughout the duration of the event. However, the IS-01 site was operational and, by that time, had been disked twice, leaving approximately 30% residue and a dust-mulch on the surface. Wind velocity profile analysis (Eq. 2) for 10-minute averages produced average u_* and $z_{0\text{-}obs}$ values of 0.462 ± 0.158 m s^{-1} and 0.003 ± 0.002 m, respectively. A plot of u_* versus u_{2m} is shown in Fig. 3. The linearity of the relationship ($r^2 > 0.86$; 95% confidence intervals shown) is clearly evident. Field observations verified soil was moving across the field but no defined saltation layer had developed. Residue conditions produced more scatter in the data compared to the 09/25/99 or 09/25/01 plots (Figs. 1 and 2) and likely due to increased turbulence and flexing of isolated, standing stubble. In addition, the IS-01 site had an additional degree of freedom (i.e. an extra anemometer in the velocity profile) used in the regression analysis. Confidence intervals indicate a good fit of the linear regression. The logarithmic wind profile conditions were confirmed in that over 90% of the profiles analyzed with Eq. 2 had r^2 values greater than 0.95 and average Ri was 0.0002 ± 0.007, indicating neutral conditions.

Saltation Roughness Height (z_{0s}):

Calculations of saltation roughness height (z_{0s}) and associated parameters by Eqs. 4, 5, 6, 7, and 8 required several pieces of information including an undisturbed z_{0u} (measured with no saltation occurring) and an estimation of available surface particle sizes most likely to saltate. Field soil ASD analysis resulted in a particle mean diameter of 45 μm, which was chosen to represent the modal surface particle size available for saltation. While this particle size is normally considered part of the suspended component for soils, it was selected to produce a conservative value for u_{*t} utilizing Eq. 6 (u_{*t} = 0.223 m s^{-1}); the u_{*t} for a 45 μm particle is slightly larger than for a 90 μm particle (u_{*t} = 0.206 m s^{-1}). Table 1 shows the size distribution results of the Ro-Tap® and sonic dry sieve analysis for Ritzville silt loam field samples. These values along with the laser diffraction results are represented in Fig. 4. Each size distribution curve indicated that the predominant particle size range was approximately between 30 μm and 60 μm. The largest particle size ranges for the sieved samples (1400 to 4000 μm) comprised nearly 10% of the sample by mass. This accounts for the shift of the sieved ASD curve to the right of the laser diffraction results. The sieved and laser-sized fractions smaller than 90 μm were approximately 66% and 80%, respectively. This is probably due to field variability and less than the +90% level seen from published soil surveys. The laser diffraction results produced more fine dust fraction due to the sample treatment methods used; fully dispersed for 1999 samples and wet suspension for 2001 samples.

Using the estimates of u_{*t} developed from the surface particle size analysis (Eq. 6), 10-minute values of z_{0s} were calculated with Eqs. 4 and 5. A representative value of z_{0u} for the 09/25/99 event was determined from a short period of high winds on 09/23/99 (16:00 to 20:15, PDT)

where wind directions was similar to the 09/25/99 event and no soil erosion or dust emissions were reported. For undisturbed conditions, the 10-minute average wind velocity at 1.5 m was 6.1 ± 1.1 m s^{-1}, and average u_* and z_{0u} were 0.409 ± 0.055 m s^{-1} and 0.004 ± 0.0004 m, respectively. The values of u_* used in Eqs. 4 and 5 were those calculated during the dust storm. Comparisons of $z_{0\text{-}obs}$, estimated z_{0s}, and $u_{1.5m}$ over the course of valid velocity profiles for the 09/25/99 wind event are shown in Fig. 5a. Early in the event and during decreasing wind speeds, $z_{0\text{-}obs}$ is slightly greater than z_{0s}. This behavior reflects the dynamics of Eq. 4 when z_0 values are relatively large (> 1 mm) and u_* values are realistic (Raupach, 1991). However, it may indicate that the velocity profile was experiencing a larger particle load than estimated with Eq. 4 and saltation was occurring. But z_{0s} consistently exceeded $z_{0\text{-}obs}$ for wind speeds greater than 10 m s^{-1}. This implies drag due to particle loads on the velocity profile was less than expected even though winds were stronger during that time. Later, when winds decreased, $z_{0\text{-}obs}$ and z_{0s} return to similar values, indicative of no saltation load (Raupach, 1991).

Values of z_{0u} for the 09/25/01 event were available from 18:00 to 22:00 (PDT) due to a very light rain (< 1 mm) that stopped all dust emissions after 18:00. The 10-minute average wind velocity for that period at 1.5 m was 6.8 ± 1.4 m s^{-1}, and average u* and z_{0u} were 0.402 ± 0.088 m s^{-1} and 0.001 ± 0.0002 m, respectively. Field observations confirmed little modification of the overall surface roughness due to the storm. Again, the values of u_* used in Eqs. 4 and 5 were 10-minute values calculated during the dust storm. The comparisons of $z_{0\text{-}obs}$, z_{0s}, and $u_{1.5m}$ for the 09/25/01 wind event are shown in Fig. 5b. Results are similar to the ’99 event except that the wind speed at which estimated z_{0s} exceeded $z_{0\text{-}obs}$ had decreased to 7.5 m s^{-1}, most likely due to the lower roughness of the W-01 site. Both graphs show z_{0s} generally exceeded $z_{0\text{-}obs}$, especially during periods of highest wind speeds, indicating that no substantial saltation was occurring during periods of highest wind speeds. Both events exhibited shifts of z_0 values during the storms. However, this was attributed to noticeable changes of wind direction, common when weather/pressure fronts pass.

In order to statistically test the differences between z_{0s} and $z_{0\text{-}obs}$, the corresponding values were sorted based on wind velocities at 1.5 m and the upper 10% from each event, 6 pair of values from the 09/25/99 event and 8 pairs from 09/25/01, representing the periods of highest wind speeds, were selected for analysis. This was justified by numerous research results showing that particle transport is intermittent in nature (Lee, 1987; Stockton and Gillette, 1990; Stout and Zobeck, 1997) and that field measurements of saltation activity have been well correlated with horizontal wind speeds (Stout and Zobeck, 1996; Sterk et al., 1998). Therefore the greatest wind speeds should correspond with the greatest saltation activity assuming no lack of saltator supply, a reasonable assumption for our field sizes. Although the total duration of the 09/25/99 event was longer then the 09/25/01 event, the number of valid wind velocity profiles was less and hence fewer readings represented the upper 10% for ’99 data. An inspection of wind speeds over the entire course of the ’99 event showed that the period examined contained the greatest sustained wind speeds. An F-test implied unequal variances and a paired T-test examined the null-hypothesis that there was no difference between the mean values of $z_{0\text{-}obs}$ and z_{0s} (Ott, 1993). The values of u, u_*, corresponding z_{0s} and $z_{0\text{-}obs}$, and the results of the statistical tests are shown in Table 2. For both events, the probability was < 0.002 that the differences between variable means was zero (i.e. the mean $z_{0\text{-}obs}$ did not equal mean z_{0s}). The C_{obs} values (Eq. 7) for the selected

$z_{0\text{-}obs}$ from each event are shown in Fig. 6 along with C_{est} (Eq. 8) for several roughness heights over a range of u_* (A = 0.22 and u_{*t} = 0.22 m s^{-1}). For each event, the C_{obs} were less than C_{est} for the observed surface roughness, approximately 0.005 m for 09/25/99 and 0.001 m for 09/25/01.

BSNE Mass Distribution:

Sonic sieve analysis of the BSNE catch from the 09/25/99 storm is shown in Fig. 7a. Few particles larger then 100 µm were trapped in the 0.1 or 0.2 m BSNEs and the particle size mode did not noticeably shift with height. The size distributions from Fig. 7a were applied to the averaged trapped BSNE mass from 12 BSNE clusters (Fig. 7b). Both the total mass and the 0-45 µm particle masses at 0.1 m were slightly less than the corresponding masses at 0.2 m. However, best-fit, two-parameter power law regressions were fitted through the 0.2 to 1.5 m data (Nickling, 1978). Mass distributions for particles larger than 45 µm allowed a two-parameter power relationship to be fit through 0.1 to 1.5 m data. The semblances of mass-height distributions for the different particle size ranges is clearly evident and indicates that similar transport processes affected the various particle size ranges.

TEOM PM_{10} Concentrations:

Continuous ambient PM_{10} concentrations were acquired during the 10/12/01 event at the IS-01 site. A time-series of 10-minute values of wind velocity at 2 m height and TEOM PM_{10} concentrations are shown in Fig. 8 ($TEOM_{1m}$ readings were only available after 11:30 PDT and readings from 14:40 to 15:20 PDT were deleted due to personnel activity at the site). From Fig. 8, it is apparent that wind speed and PM_{10} concentrations were well correlated. Correlation coefficients (r) were calculated for PM_{10} readings and velocities at each anemometer height (Table 3) from 11:30 to 16:30 PDT, the time when PM_{10} concentrations were rapidly increasing. The r values for the $TEOM_{1m}$ ranged from 0.60 to 0.75 and $TEOM_{3m}$ r values ranged from 0.55 to 0.68. All correlations were highly significant with 27 observations (Taylor, 1982). Spearman's rank order correlation coefficients (r_s) were > 0.91 for each TEOM at all anemometer heights (Ott, 1993). Correlations with the velocities from the lower anemometers and the rapid changes in $TEOM_{1m}$ PM_{10} readings suggest that a significant portion of the PM_{10} came from the IS-01 site. However, $TEOM_{3m}$ output lagged the velocity spike at 14:00 and both TEOMs lagged the latter velocity peak (approximately 17:20) by about one hour, indicating some influence from upwind PM_{10} sources.

Discussion:

Observation and verification of the saltation effect on velocity profiles has been previously documented theoretically, experimentally in wind tunnels, and in the field. Therefore, modified velocity profiles should be observed in our research field sites if significant saltation loads were occurring. As noted earlier, prior field studies have documented intermittent saltation (Lee, 1987; Stockton and Gillette, 1990; Stout and Zobeck, 1997). However, the constancy of the drag coefficient (C_d: Eq. 1) displayed by the similarity and linearity of u_* versus u for 10-minute and 1-minute results of the 09/25/99 and 09/25/01 wind events (Figs. 1 and 2) indicate that little saltation took place. In addition, the location of the W-01 site (bordering large sand dunes) would be expected to have sand-sized particles available for saltation.

Velocity profiles may also be affected by atmospheric stability conditions due to heating and thermal gradients (Frank and Kocurek, 1994). However, the low Ri values and dominance of

logarithmic velocity profiles indicates that neutral conditions prevailed during substantial portions of the high wind events analyzed. This was expected because the events occurred under generally cloudy conditions and high turbulence.

Plots of $z_{0\text{-obs}}$ and z_{0s} for the 1999 and 2001 wind events (Fig. 5) show substantial periods where estimates of z_{0s} were greater than $z_{0\text{-obs}}$, indicating that saltation increase of z_0 was not observed. There are periods when the trend is not sustained, notably at slower wind speeds. Considering that Gillette et al. (1998) recommended a larger coefficient A (= 0.38) for Eq. 4, it could be argued that z_{0s} were generally underestimated. In that case, there would be longer periods when estimated z_{0s} were greater than $z_{0\text{-obs}}$, also indicating that little saltation occurred. The 1999 event showed a slight increase of z_0 when comparing z_{0u} (undisturbed conditions) and $z_{0\text{-obs}}$. However, the increase could easily be attributed to other factors including slight changes in wind directions or surface conditions. Arguments could also be made that the modal surface particle size (45 μm) was too small to represent saltating particles. However, numerous studies have shown minimum u_{*t} values occur with particles approximately 80 μm in diameter, with higher u_{*t} values for larger and smaller particles (Greeley and Iversen, 1985). The 45 μm u_{*t} also corresponds to u_{*t} for particles 130 μm in diameter, a common saltator-sized particle over a wide range of erodible soils (Gillette and Chen, 1999). Therefore, the estimation of z_{0s} holds for saltator-sized particles. Additional estimations of z_{0s}, with u_{*t} (Eq. 6) and r (Eq. 5) calculated for particles in the 45 to 130 μm range, showed little change of trends shown in Fig. 5. A limited supply of saltator-sized particles (Lopez, 1998) could explain some of the early trends seen in Fig. 5a but, as noted earlier, was unlikely due to the large field size. The comparison of C_{obs} and C_{est} (Fig. 6; Eqs. 7 and 8) also shows that the observed roughness heights were less than predicted and that little saltation took place.

The particle size distribution with height analysis displayed further evidence that suspension processes dominated particle transport. Although the resolution between size ranges was less than ideal, the modal size peak remained at 10 to 45 μm (Fig. 7a) for all BSNE heights. This contrasted with other studies that noted large modal shifts in particle sizes with height (Leys and McTainsh, 1996; Gillette et al., 1997). Limited laser sizing (weakly dispersed) of BSNE catch from more recent storms showed a similar trend (Kjelgaard, unpublished data) with median particle size ranging from 39 to 25 μm and unimodal particle diameter peak shifting from approximately 60 to 30 μm as sampling height increased from 0.1 to 1.5 m. Scanning electron microscope (SEM) images of loose surface particles up to 125 μm mean diameter revealed flat, platy, and angular particle structures consistent with the glacial and volcanic sources of the loess material (Kjelgaard, unpublished data). Rice (1991), in wind tunnel studies, found that particles with reduced sphericity were more likely to be aerodynamically entrained, less likely to saltate, and if saltation occurred, less energetic in subsequent rebounds with the surface (i.e. reduced sand-blasting effect).

Overall, the percentages of particles with mean diameters larger then 100 μm was extremely small at all sampling heights and displays an overall lack of traditional saltation-sized particles on the surface. The low percentage of particles with diameters < 10 μm can be attributed to inefficiencies of the BSNE with small particles (Shao et al., 1993; Goosens and Offer, 2000). As noted, the resemblance of particle distributions from 0.2 to 1.5 m for different diameter ranges supports the notion that the transport processes were similar (Fig 7b). Leys and McTainsh (1996)

found separate functions described total particle mass and mass for particles smaller than 90 μm, respectively, for erosion-prone soils in Australia. The similarity of total mass caught at 0.1 and 0.2 m was not noted in prior field studies on the Columbia Plateau (Stetler et al., 1994; Stetler and Saxton, 1996). However, all the wind events they examined, with one exception, had average BSNE catch < 1.3 g at 1.5 m, much less then the 09/25/99 (approximately 6 g average in 1.5 m BSNE) or 09/25/01 (approximately 9.5 g average in 1.5 m BSNE) events. Assuming the direct suspension of larger particles would still limit their maximum trajectory height to < 30 cm (Gillette et al., 1997), the 0.1 m BSNE would sample a smaller "footprint" area for particles to be emitted from compared to the 0.2 m BSNE.

Examination of TEOM measurements from the 10/12/01 wind event (Fig. 8) showed concentrations of PM_{10} increased rapidly when wind velocities were above 8 m s^{-1}. A value of u_{*t} for PM_{10} (0.579 m s^{-1}) was calculated with Eq. 6 and $z_{0\text{-}obs}$ (0.003 ± 0.0022 m) were substituted into Eq. 2. The corresponding threshold velocity (u_t) at 2 m was 9.4 m s^{-1} with a range, based on $z_{0\text{-}obs}$, of 8.6 m s^{-1} to 11.3 m s^{-1}. Though the data is limited, these results indicate that direct wind energy was likely the primary entrainment force because larger particles available for saltation would have required a lower u_{*t} than that estimated with Eq. 6. For example, a 90 μm particle has a u_{*t} = 0.206 m s^{-1} and a corresponding $u_t \approx 3.4$ m s^{-1} at 2 m (Eq. 2) under identical roughness conditions. If larger particles had been saltating, abrading, or ejecting smaller particles via surface collisions, rising PM_{10} levels would be expected at much lower threshold wind speeds than those observed, especially with a loose, disaggregated field surface. Kjelgaard and Rude (manuscript submitted for review), using TEOM data, found that residue cover had a minimal effect on the apparent threshold velocity for PM_{10} on Ritzville series soils. They examined PM_{10} emissions from the IS-01 site from the 10/12/01 event and a subsequent event approximately one year later. Despite significant reductions in residue and surface clods, substantial increases in PM_{10} occurred at approximately 8 m s^{-1} for both years, although there were large differences in relative PM_{10} concentrations.

Conclusions:

The Columbia Plateau, located in north-central Oregon and south-central Washington, is a region with extensive loess deposits where up to 90% of particles (by weight) have diameters less than 100 μm. The most susceptible soils, Ritzville series, contain few saltator-sized particles by dry sieve analysis (70-500 μm mean particle diameter) readily available on the soil surface and little evidence of observed saltation layers or deposition during high wind events. This suggests that saltation is not likely a major erosion or entrainment process.

Velocity profile analyses of two major high wind dust events and one minor dust event provided evidence that there was little modification of the wind profile due to saltation loads. Graphs of u_* versus u were very linear, indicating little change in surface roughness for the wind events. The linearity is quite different from the curvilinear relationship found at Owens Lake by Gillette et al. (1997 and 1998) where a strong saltation layer existed. For our fields, comparisons of an estimated z_{0s} and $z_{0\text{-}obs}$, based on wind velocity profiles, showed extensive high wind periods when $z_{0\text{-}obs}$ was less than z_{0s}, indicating little or no saltation load on the velocity profile.

Examination of particle mass and size distributions with height from event-averaged BSNE measurements for the 09/25/99 wind event showed no shift of modal particle range with height

from 0.1 to 1.5 m. The distribution of mass based on mean particle diameters were similar for the diameter size ranges examined.

Data from continuous PM_{10} monitors (TEOMs) located on an intensive wind erosion study site showed minimal elevated PM_{10} concentrations prior to their expected threshold as estimated with the equation of Marticorena and Bergametti (1995). Had there been a significant amount of larger particles in saltation, finer particles would likely have been dislodged through surface bombardment or particle abrasion and increased PM_{10} levels at lower wind velocities.

The detailed analysis of wind velocity profiles, surface roughness, BSNE catch, and TEOM data substantiates that saltation is a very small component of wind erosion for fine, silt loam soils of the Columbia Plateau. Soil entrainment is dominated by suspension processes. Wind erosion and dust emission algorithms need to account for this when modeling or measuring soil losses in this region.

Acknowledgements

The authors would like to acknowledge the technical assistance of Robert Barry with various aspects of field and laboratory research. Dr. Alan Busacca's lab conducted the laser particle size analysis. The comments and questions from our reviewers were greatly appreciated. Funds for the research were provided by the USDA-ARS CP3 Project. Additional resources were provided by Washington State University. Products or manufacturers mentioned in the text are not endorsed by participating institutions or agencies.

References

Anderson RS, Haff PK. 1991. Wind modification and bed response during saltation of sand in air. Acta Mech. 1:21-51.

Bagnold RA. 1941. *The physics of blown sand and desert dunes*. Methuen, New York, New York. pps. 265.

Borrmann S, Jaenicke R. 1987. Wind tunnel experiments on the resuspension of sub-micrometer particles from a sand surface. Atmos. Environ. 21:1891-1898.

Cahill TA, Gill TE, Reid JS, Gearhart EA, Gillette DA. 1996. Saltating particles, playa crusts and dust aerosols at Owens (dry) lake, California. Earth Surf. Processes and Landforms. 21:621-639.

Chepil WS. 1945. Dynamics of wind erosion II: initiation of soil movement. Soil Sci. 60:397-411.

Frank A, Kocurek G. 1994. Effects of atmospheric conditions on wind profiles and Aeolian sand transport with an example from White Sands national monument. Earth Surf. Processes and Landforms. 19:735-745.

Fryear DW. 1986. A field dust sampler. J. Soil and Water Cons. 41:117-119.

Gillette DA, Walker TR. 1977. Characteristics of airborne particles produced by wind erosion of sandy soil, high plains of west Texas. Soil Sci. 123:97-110.

Gillette DA, Herbert G, Stockton PH, Owen PR. 1996. Causes of the fetch effect in wind erosion. Earth Surf. Processes and Landforms. 21:641-659.

Gillette DA, Hardebeck E, Parker J. 1997. Large-scale variability of wind erosion mass flux rates at Owens Lake: 2. Role of roughness change, particle limitation, change of threshold friction velocity, and the Owen effect. J. Geophy. Res. 102:25989-25998.

Gillette DA, Marticorena B, Bergametti G. 1998. Change in the aerodynamic roughness height by saltating grains: Experimental assessment, test of theory, and operational parameterization. J. Geophy. Res. 103:6203-6209.

Gillette DA, Chen W. 1999. Size distributions of saltating grains: an important variable in the production of suspended particles. Earth Surf. Processes and Landforms. 24:449-462.

Goosens D, Offer ZY. 2000. Wind tunnel and field calibration of six aeolian dust samplers. Atmos. Environ. 34:1043-1057.

Greeley R, Iversen JD. 1985. *Wind as a geological process on Earth, Mars, Venus, and Titan*. Cambridge University Press. New York, New York. pps. 333

Houser CA, Nickling WG. 2001. The emission and vertical flux of particulate matter < 10 μm from a disturbed clay-crusted surface. Sediment. 48:255-267.

Iversen JD, Pollack JB, Greeley R, White BR. 1976. Saltation threshold on Mars: the effect of interparticle force, surface roughness, and low atmospheric density. Icarus. 29:381-393.

Kaimal JC, Finnigan JJ, 1994. *Atmospheric boundary layer flows, their structure and measurement.* Oxford University Press. New York, New York. pps. 289

Kind RJ. 1992. Concentration and mass flux of particles in aeolian suspension near tailings disposal sites or similar sources. J. Wind Eng. and Industr. Aerodynamics. 41-44:217-225.

Lee JA. 1987. A field experiment on the role of small scale wind gustiness in aeolian sand transport. Earth Surface Processes and Landforms. 12:331-335.

Leys JF, McTainsh GH. 1996. Sediment fluxes and particle grain-size characteristics of wind-eroded sediments in southeastern Australia. Earth Surface Processes and Landforms. 21:661-671.

Ling CH. 1976. On the calculation of surface shear stress using the profile method. J. Geophy. Res. 81:2581-2582.

Loosmore GA, Hunt JR. 2000. Dust resuspension without saltation. J. Geophy. Res. 105:20663-20671.

Lopez MV. 1998. Wind erosion on agricultural soils: an example of limited supply of particles available for erosion. Catena. 33:17-28.

Marticorena B, Bergametti G. 1995. Modeling the atmospheric dust cycle: 1. Design of a soil-derived dust emission scheme. J. Geophy. Res. 100:16415-16430.

Nickling WG. 1978. Eolian sediment transport during dust storms: Slims River Valley, Yukon Territory. Can. J. Earth Sci. 15:1069-1084.

Nickling WG. 1983. Grain-size characteristics of sediment transported during dust storms. J. Sed. Petrology. 53(3):1011-1024

Ott RL. 1993. *An introduction to statistical methods and data analysis*. Duxbury Press. Belmont, California. pps. 1183

Owen PR. 1964. Saltation of uniform grains in air. J. Fluid Mech. 20:225-242.

Pye K. 1987. *Aeolian dust and dust deposits*. Academic Press. New York, New York. pps. 334

Raupach MR. 1991. Saltation layers, vegetation canopies and roughness lengths. Acta Mech. 1:83-96.

Rice MA. 1991. Grain shape effects on aeolian sediment transport. Acta Mech. 1:159-166.

Sagan C, Bagnold RA. 1975. Fluid transport on Earth and aeolian transport on Mars. Icarus. 26:209-218.

Saxton KE. 1995. Wind erosion and its impact on off-site air quality in the Columbia Plateau – an integrated research plan. Trans. ASAE. 38(4):1031-1038.

Saxton KE, Chandler D, Stetler L, Lamb B, Claiborn C, Lee BH. 2000. Wind erosion and fugitive dust fluxes on agricultural lands in the Pacific Northwest. Trans. ASAE. 43(3):623-630.

Shao Y. 2001a. A model for mineral dust emission. J. Geophy. Res. 106:20239-20254.

Shao Y. 2001b. *Physics and modelling of wind erosion*. Kluwer Academic Publishers. Boston, Massachusetts. pps. 393.

Shao Y, Raupach MR, Findlater PA. 1993. Effect of saltation bombardment on the entrainment of dust by wind. J. Geophy. Res. 98:12719-12726.

Sterk G, Spaan WP. 1997. Wind erosion control with crop residues in the Sahel. Soil Sci. Soc. Am. J. 61:911-917.

Sterk G, Jacobs AFG, Van Boxel JH. 1998. The effect of turbulent flow structures on saltation sand transport in the atmospheric boundary layer. Earth Surface Processes and Landforms. 23:877-887.

Stetler LD, Saxton KE. 1996. Wind erosion and PM_{10} emissions from agricultural fields on the Columbia Plateau. Earth Surface Processes and Landforms. 21:673-685.

Stetler LD, Saxton KE, Fryrear DW. 1994. Wind erosion and PM_{10} measurements from agricultural fields in Texas and Washington. Annual Meeting Technical Papers, no. 94-FA145.02, *Air and Waste Manag. Assoc.'s 87th Annual Meeting & Exhibition,* June 19-24, Cincinnati, OH, 14 pps.

Stockton P, Gillette DA. 1990. Field measurements of the sheltering effect of vegetation on erodible land surfaces. Land Degradation and Rehab. 2:77-85.

Stout JE. 1990. Wind erosion within a simple field. Trans. ASAE 33(5):1597-1600.

Stout JE, Zobeck TM. 1996. The Wolfforth field experiment: a wind erosion study. Soil Sci. 161:616-632.

Stout JE, Zobeck TM. 1997. Intermittent saltation. Sediment. 44:959-970.

Stull R. 2000. *Meteorology for scientists and engineers (2nd edition).* Brooks/Cole. Pacific Grove, California. pps. 502.

Taylor J. 1982. *An introduction to error analysis: the study of uncertainties in physical measurements*. University Science Books. Mill Valley, California. pps. 270.

Thom AS. 1975. Momentum, mass and heat exchange of plant communities. In Monteith JL (Ed.), *Vegetation and the atmosphere,* Academic Press. New York, New York. pps. 57-109.

U.S. D. A. 1967. Soil survey: Adams County, Washington. p. 102.

U.S. E. P. A. 1990. Clean air act amendments of 1990, detailed summary of titles, title 1-provisions for attainment and maintenance of national ambient air quality standards-ozone, carbon monoxide, and PM_{10} nonattainment provisions. pps. 24-28.

White BR. 1982. Two-phase measurements of saltating turbulent boundary layer flow. Int. J. Multiphase Flow. 5:459-473.

Zingg AW. 1953. Wind tunnel studies of the movement of sedimentary material. Proceedings 5th Hydraulic Conference Bulletin. 34:111-135.

Zobeck TM, Fryrear DW. 1986. Chemical and physical characteristics of windblown sediment II. chemical characteristics and total soil and nutrient discharge. Trans. ASAE. 29:1037-1041.

Kjelgaard J
Top, Table 1

Particle Diameter Range (μm)	Average Mass (%)	Standard Deviation (%)
< 10	1.0	0.5
10 – 30	14.0	6.3
30 – 45	20.6	11.4
45 -63	16.6	12.1
63 – 90	13.5	7.0
90 – 125	8.6	0.7
125 – 180	7.0	2.0
180 – 250	2.5	2.9
250 – 355	3.1	2.1
355 – 500	0.9	2.0
500 – 710	0.4	1.9
710 – 1000	0.1	2.0
1000 – 1400	0.0	2.0
1400 – 2000	0.4	2.0
2000 – 4000	4.7	1.5
> 4000	6.2	0.3

Table 1. Percentage of mass for particle size ranges averaged for 3 sites of Ritzville Silt Loam surface soils using Ro-Tap® and sonic dry sieve analysis.

Kjelgaard J
Top, Table 2

	09/25/99 Event			
	u @ 1.5m ($m\ s^{-1}$)	u* ($m\ s^{-1}$)	$z_{0\text{-}obs}$ (mm)	z_{0s} (mm)
	11.7	0.803	4.8	6.1
	11.6	0.804	5.0	6.2
	11.5	0.803	5.1	6.1
	11.4	0.831	6.1	6.5
	11.4	0.787	5.1	5.9
	11.2	0.773	4.7	5.8
Average	11.5	0.800	5.1	6.1
St. Dev.	0.2	0.019	0.5	0.2
F-test probability that variance z_0 = variance z_{0s} < 0.12				
T-test probability that mean z_0 - mean z_{0s} = 0 < 0.002				
	09/25/01 Event			
	u @ 1.5m ($m\ s^{-1}$)	u* ($m\ s^{-1}$)	$z_{0\text{-}obs}$ (mm)	z_{0s} (mm)
	13.8	0.874	2.3	5.4
	13.4	0.843	2.1	5.0
	13.4	0.854	2.4	5.2
	13.1	0.823	2.2	4.8
	12.8	0.798	2.1	4.5
	12.7	0.782	2.0	4.4
	12.2	0.754	1.9	4.1
	12.2	0.756	2.1	4.1
Average	12.9	0.810	2.1	4.7
St. Dev.	0.6	0.045	0.2	0.5
F-test probability that variance z_0 = variance z_{0s} < 0.007				
T-test probability that mean z_0 - mean z_{0s} = 0 < 0.001				

Table 2. Upper 10% of 10-minute, 1.5 m wind speeds (u) from the 09/25/99 and 09/25/01 wind events (representing the events' greatest wind velocities), corresponding friction velocities (u_*), observed roughness heights ($z_{0\text{-}obs}$), estimated saltation roughness heights (z_{0s}), and results of statistical tests.

Kjelgaard J
Top, Table 3

	Anemometer Heights (m)					
	0.1	0.5	1.0	2.0	3.0	5.0
$TEOM_{1m}$	0.60	0.70	0.68	0.68	0.71	0.75
$TEOM_{3m}$	0.55	0.63	0.62	0.61	0.62	0.68

Table 3. Correlation coefficients (r) between 10-minute interval TEOM PM_{10} concentrations and wind velocities, IS-01 site, between 11:30 and 16:30 PDT (n = 27), 10/12/01 wind event.

Figure Captions

Figure 1. Friction velocity (u_*) versus wind velocity at 1.5 m ($u_{1.5m}$) from 09/25/99 dust event, R-99 site: a) 10-minute averaged values, b) 1-minute averaged values, u_* based on analysis of the lowest 2 anemometers, 0.1 m and 0.75 m.

Figure 2. Friction velocity (u_*) versus wind velocity at 1.5 m ($u_{1.5m}$) from 09/25/01 dust event, W-01 site: a) 10-minute averaged values, b) 1-minute averaged values, u_* based on analysis of the lowest 2 anemometers, 0.1 m and 1.5 m.

Figure 3. Ten minute averaged values of friction velocity (u_*) versus wind velocity at 2 m (u_{2m}) from 09/25/01 dust event, IS-01 site.

Figure 4. Aggregate size distribution for Ritzville silt loam surface soil samples by mechanical sieving and dispersed laser diffraction.

Figure 5. Wind velocity at 1.5 m ($u_{1.5m}$), roughness height (z_0), and saltation roughness height (z_{0s}), over time (PDT) a) 09/25/99 dust event, R-99 site, b) 09/25/01 dust event, W-01 site.

Figure 6. Values of C_{est} (Eq. 8) for selected roughness heights and friction velocities (A = 0.22, $u_{*t} = 0.22$ m s^{-1}), and values of C_{obs} (Eq. 7) from measurements during 09/25/99 and 09/25/01 wind events, based on Table 3 results.

Figure 7. a) Particle size distribution of loose surface soils and BSNE catch from 09/25/99 wind event, b) BSNE mass distribution with height for all particles, particles with mean diameter > 45 μm, and particles with mean diameters < 45 μm.

Figure 8. Wind velocity at 2 m (u_{2m}) and PM_{10} concentrations at 1 m and 3 m over time (PDT) for the 10/12/01 dust event, IS-01 site.

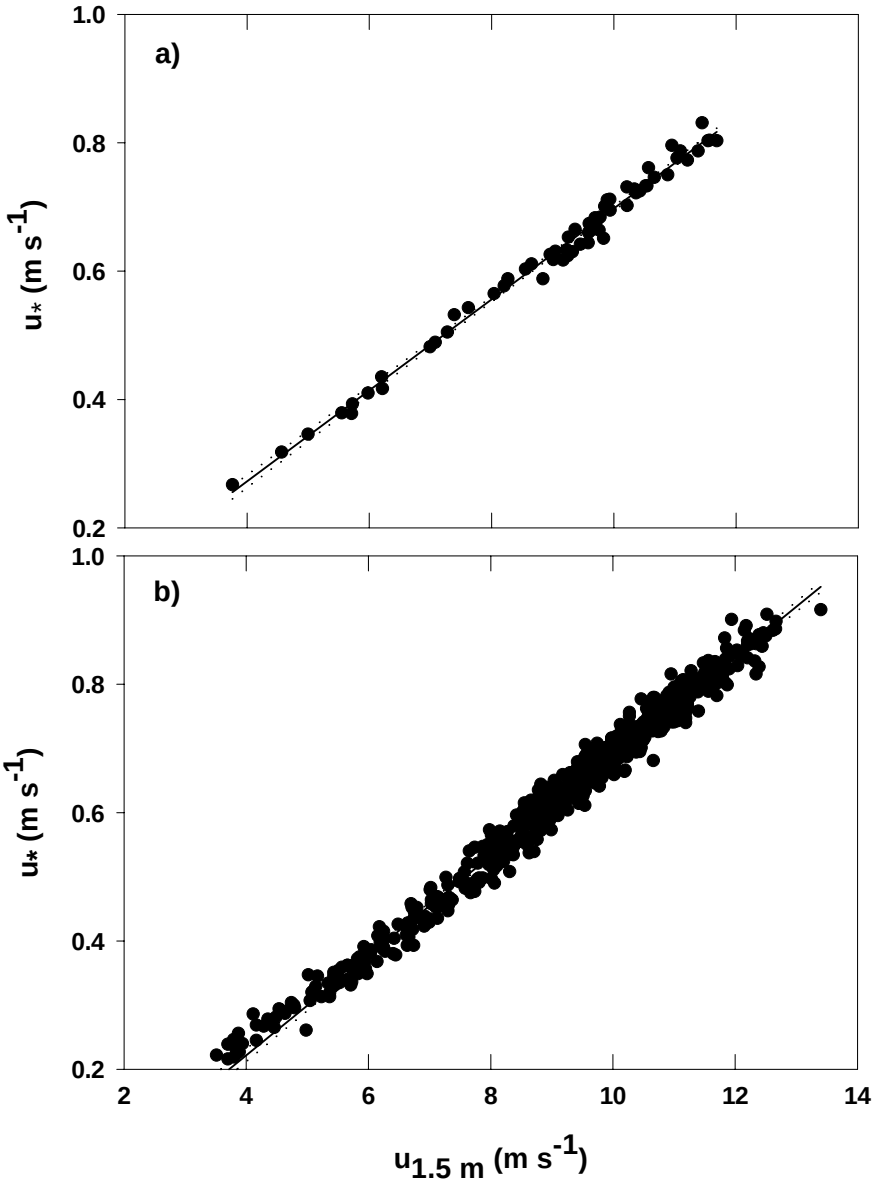

J. Kjelgaard
Figure 1, Bottom

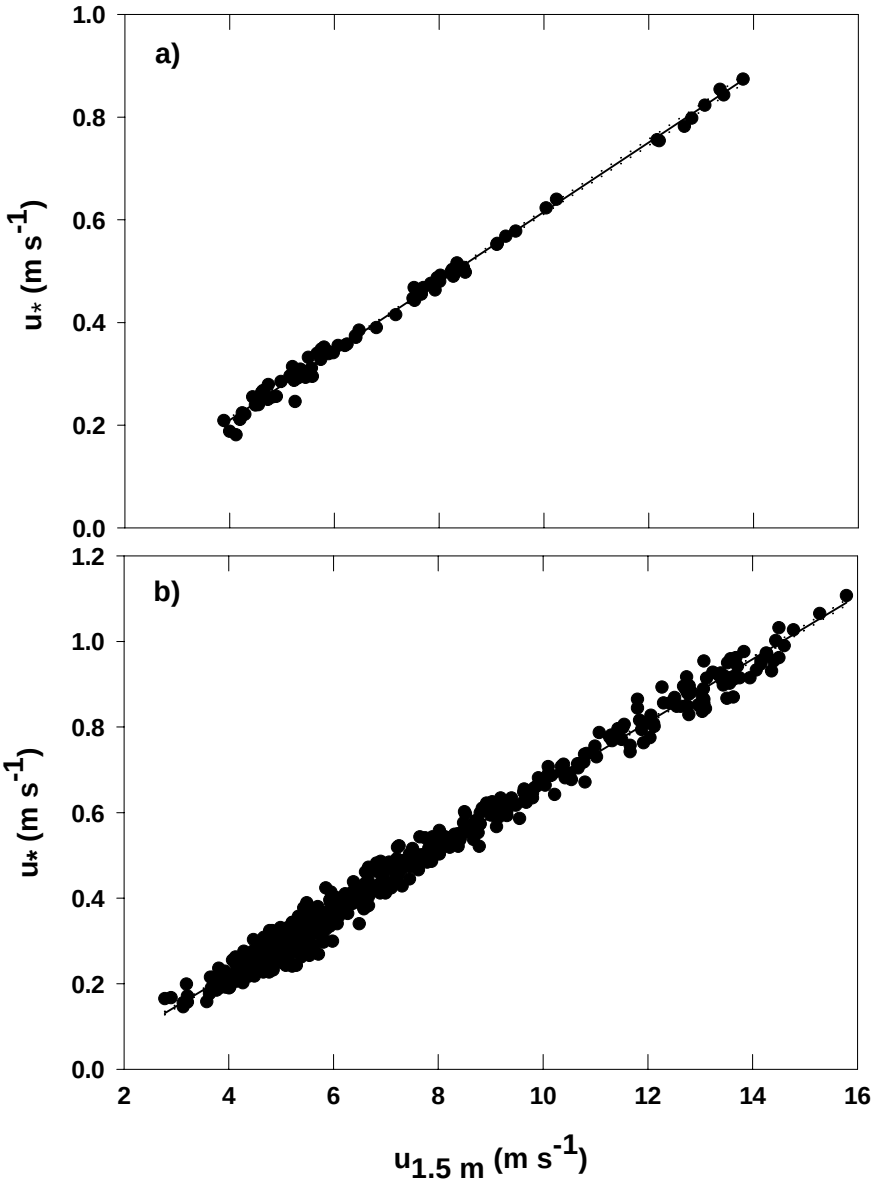

J. Kjelgaard
Figure 2, Bottom

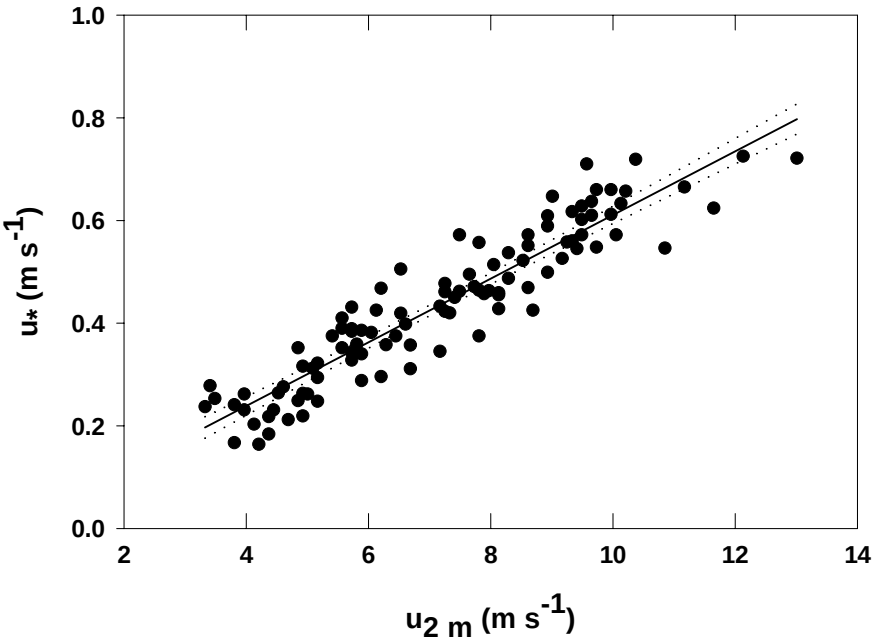

J. Kjelgaard
Figure 3, Bottom

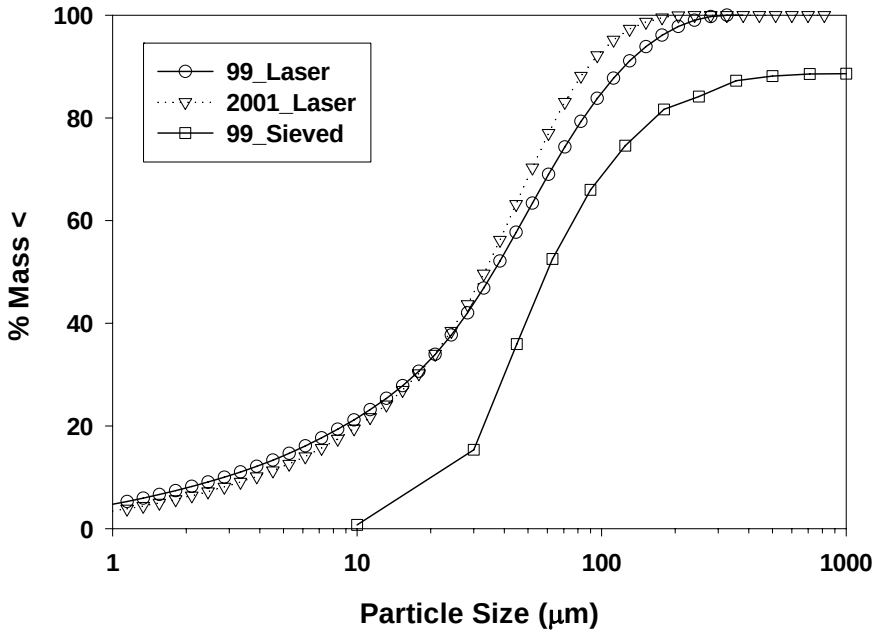

J. Kjelgaard
Figure 4, Bottom

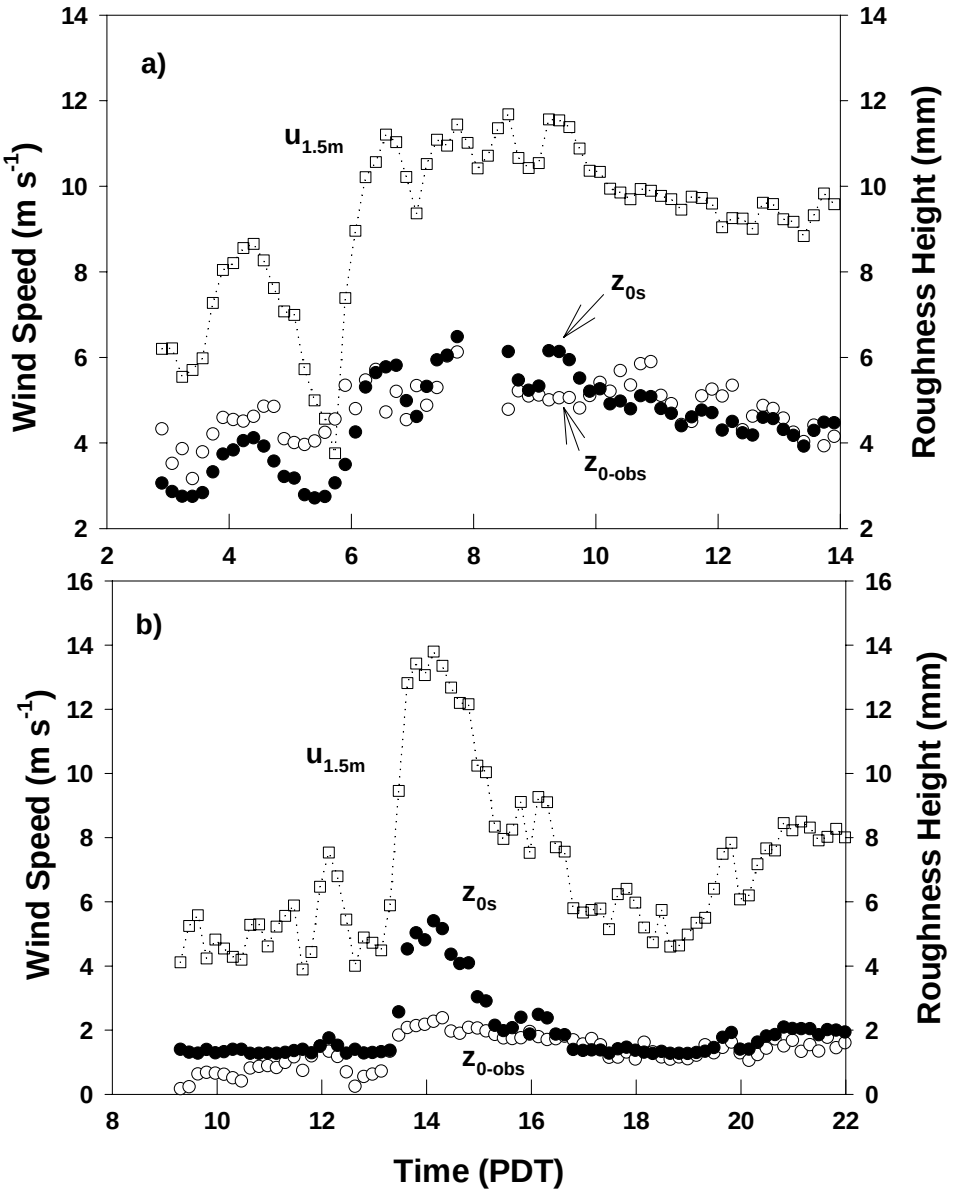

J. Kjelgaard
Figure 5, Bottom

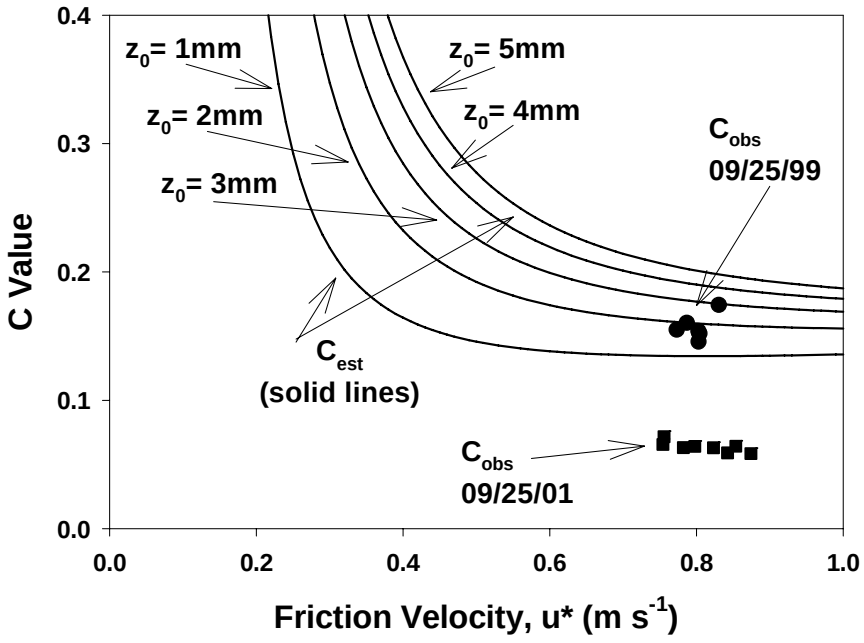

J. Kjelgaard
Figure 6, Bottom

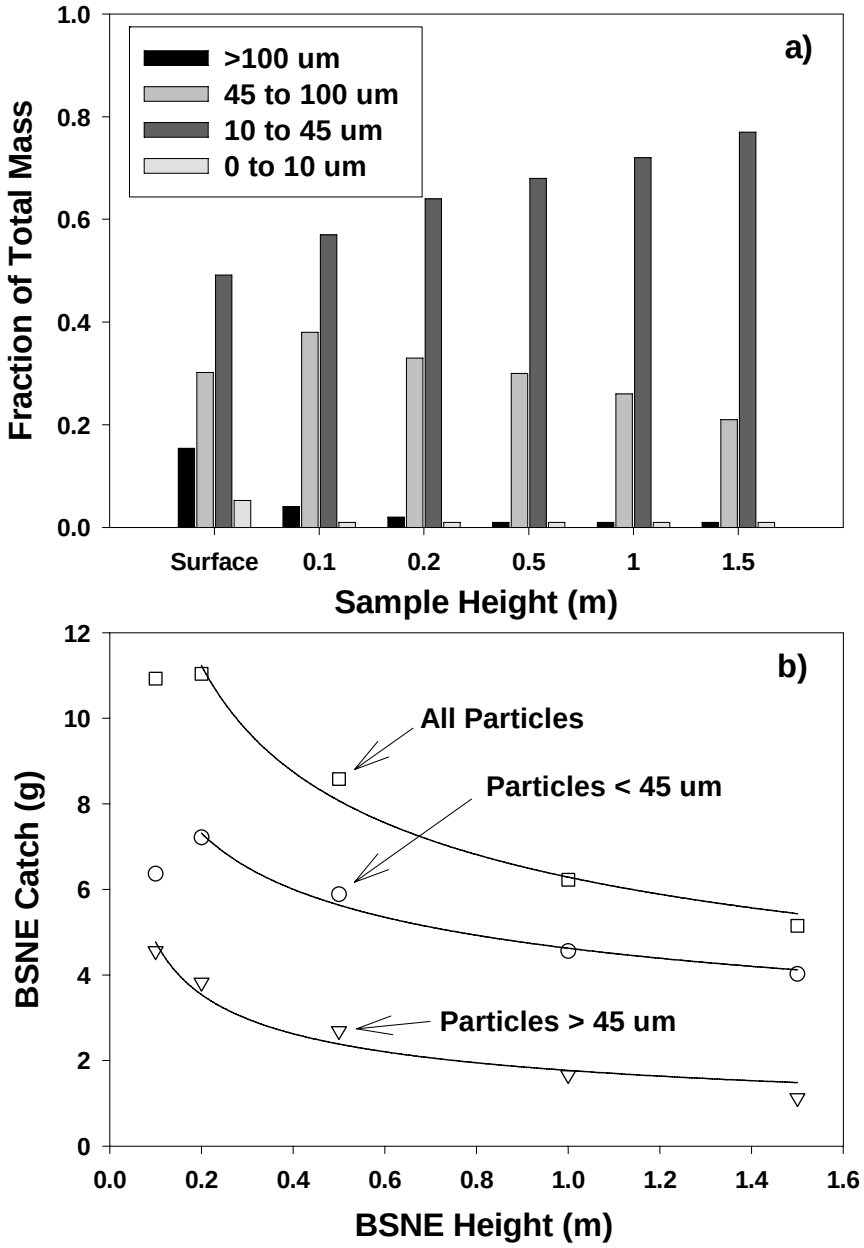

J. Kjelgaard
Figure 7, Bottom

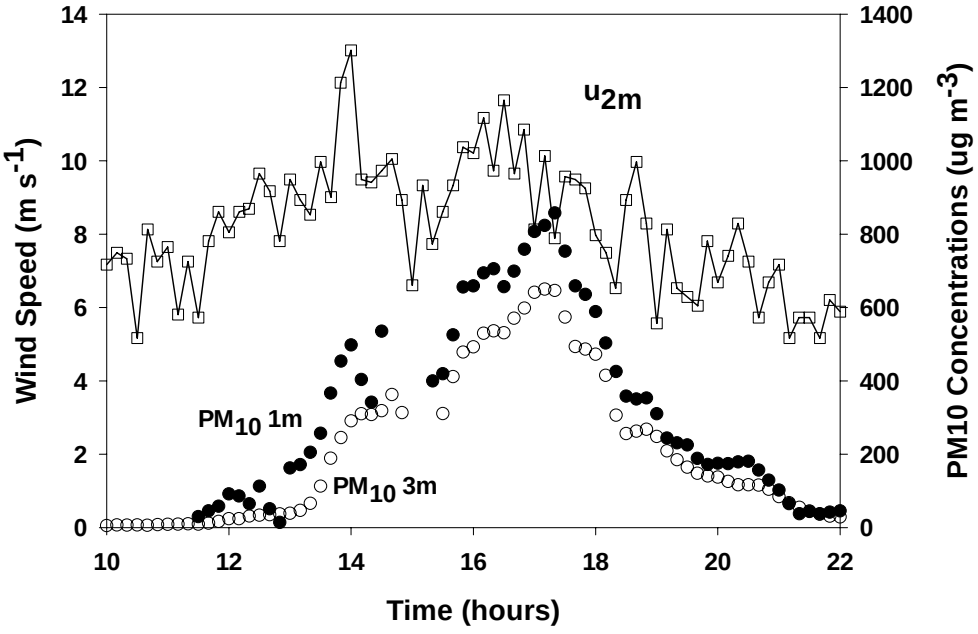

J. Kjelgaard
Figure 8, Bottom